DOI: 10.24352/UB.OVGU-2017-107 TECHNISCHE MECHANIK, 37, 2-5, (2017), 314 – 325
submitted: April 12, 2017

Reduced Order Modeling of Mistuned Bladed Disks under Rotation

S. Willeke, L. Panning-von Scheidt, J. Wallaschek

In this paper, a substructure-based reduced order model for mistuned bladed disks is extended to account for the effect of rotational-dependent dynamic properties. To reduce the overall size of the structural model, successive transformations to reduced modal subspaces of smaller dimension are performed by means of a fixed-interface Component Mode Synthesis, a Wave-Based Substructuring, and a Secondary Modal Truncation. Since the three-dimensionally shaped rotor blades tend to untwist under the influence of centrifugal forces, the modal reduction bases may undergo significant changes for different speeds of rotation. To prevent the necessity of identifying individual modal subspaces for each operating point and a repetitious passing through the full reduction process, a multi-model formulation is used to obtain a parameterized reduced order model in terms of rotational speed. The accuracy of this approach is assessed by comparison with full finite element models for various steady operating conditions. In terms of computational solution time, the proposed approach outperforms the finite element calculation by 90%. Finally, numerical results are presented addressing the mitigating influence of constant and variable rotational speeds on the amplitude amplification of mistuned bladed disks.

1 Introduction

During operation, the rotating bladed disks in turbomachines are exposed to large static and dynamic stresses. While static loads mainly arise from centrifugal forces and thermal strains, fluctuating gas pressures and rotor imbalances lead to forced vibrations. In particular, the periodic motion of the rotor blading through the irregular wake pattern downstream the stator vanes is known as a major source of forced excitation. Besides this synchronous stimulus, unsteady flow phenomena like aeroelastic flutter may cause self-excited blade vibrations of asynchronous type. The response of the structural components to these forcing mechanisms is in turn affected by the rotational motion. For instance, the static stresses stemming from centrifugal forces change the frequency characteristic of the rotating structure. In addition, small imperfections caused by the manufacturing process break the cyclic symmetry of the bladed disk and lead to a local concentration of vibrational energy. This mistuning may cause increased blade vibration amplitudes which in turn lead to an elevated risk of high-cycle fatigue. To efficiently predict this amplitude amplification in the turbomachinery design process, *Reduced Order Models* (ROM) of the full annulus are applied.

A numerical comparison between the mistuned vibrations of a transonic shrouded fan at 8,000 rpm and at rotor rest is presented in Moyroud et al. (2002). It is concluded from simulations that the stiffening effect of the rotational motion mitigates stiffness perturbations between the blades and reduces the overall sensitivity to mistuning. To approximate the evolution of mistuning under the influence of rotation, a simplified prediction method is proposed by Feiner (2002) and by Feiner and Griffin (2004). In combination with the *Fundamental Mistuning Model* (FMM), it is used to predict the response of an integrally bladed compressor disk at 40,000 rpm. A similar method for the approximation of the mistuned blade stiffness under rotation is described by Nipkau (2011) based on an SDOF-approach. Its application in numerical studies of a high pressure compressor blisk indicates a reduced effect of mistuning under rotation. Experimental measurements of a mistuned centrifugal impeller by Maywald et al. (2009) show no significant influence of rotation on mistuning for a speed range from 10,000 rpm to 19,000 rpm. A reduced multi-model approach that allows to consider mistuning under rotation is presented by Balmès (1996), Sternchüss and Balmès (2008), and Sternchüss (2009).

The present paper focuses on the extension of a substructure-based reduced order approach described in Hohl et al. (2009) by the multi-model formulation proposed in Balmès (1996), Sternchüss and Balmès (2008), and Sternchüss (2009). To this end, the modal subspaces of each reduction step are enriched by additional modes at various operating points in the analyzed range of rotational speeds. In addition, the effect of stiffness variation by centrifugal forces on the associated natural frequencies is incorporated by a second-order polynomial in the structural stiffness matrix (Sternchüss, 2009).

In order to predict the forced response of a mistuned bladed disk at an angular frequency ω, the following equation of motion at the rotational speed Ω is solved:

$$\left[-\omega^2\mathbf{M} + \mathrm{i}\omega\mathbf{C}_\mathrm{v}\left(\Omega\right) + \mathrm{i}\mathbf{C}_\mathrm{s}\left(\Omega\right) + \mathbf{K}\left(\Omega\right)\right]\hat{\mathbf{u}} = \hat{\mathbf{f}}_\mathrm{e}\,. \tag{1}$$

Since the present study is focused on modeling the interacting effects of centrifugal stiffness variations and structural mistuning, any gyroscopic effects in Eq. (1) are neglected. Proportional and structural damping $\mathbf{C}_\mathrm{v}$ and $\mathbf{C}_\mathrm{s}$ are considered in terms of the mass matrix $\mathbf{M}$ and the stiffness matrix $\mathbf{K}$,

$$\mathbf{C}_\mathrm{v}\left(\Omega\right) = \alpha\mathbf{M} + \beta\mathbf{K}\left(\Omega\right) \qquad \text{and} \qquad \mathbf{C}_\mathrm{s}\left(\Omega\right) = d_0\mathbf{K}\left(\Omega\right)\,. \tag{2}$$

The vectors $\hat{\mathbf{u}}$ and $\hat{\mathbf{f}}_\mathrm{e}$ denote the displacement and forcing amplitudes of each blade k respectively,

$$\mathbf{u} = \hat{\mathbf{u}}\mathrm{e}^{\mathrm{i}(\omega t+\phi_\mathrm{u})} \quad \text{and} \quad \mathbf{f}_\mathrm{e} = \hat{\mathbf{f}}_\mathrm{e}\mathrm{e}^{\mathrm{i}(\omega t+\phi_\mathrm{e})} \quad \text{where} \quad \phi_{\mathrm{e,k}} = \frac{2\pi}{N}\mathrm{EO}\,(k-1) \quad \text{for} \quad k = 1,\,2,\,\ldots,\,N\,. \tag{3}$$

In case of synchronous excitation mechanisms, the angular forcing frequency ω is expressed in terms of the *Engine Order* (EO) and the rotational speed Ω as

$$\omega = \mathrm{EO}\cdot\Omega\,. \tag{4}$$

Depending on the finite element discretization of the structure, the vector $\hat{\mathbf{u}}$ may contain numerous degrees of freedom. To reduce the computational effort for solving Eq. (1), the problem is projected to modal subspaces of gradually smaller dimensions.

2 Reduced Order Modeling of mistuned bladed Disks

In this section, the substructure-based reduction technique presented by Hohl et al. (2009) is summarized prior to addressing its multi-model extension. The reduction steps include a *Component Mode Synthesis* (CMS), a *Wave-Based Substructuring* (WBS), and a *Secondary Modal Truncation* (SMT).

2.1 Component Mode Synthesis

Based on the finite element representation of a single segment, the bladed disk is partitioned into a cyclic symmetric disk and the mistuned blading components. By distinguishing degrees of freedom along the blade-disk-interface boundary Γ from the internal domain Ξ, the matrix $\mathbf{Z}$ related to a component s (i.e. either a blade or the disk) at operating point $n \in \mathbb{N}$ is described by,

$$\mathbf{Z}^{(s,n)} = \begin{bmatrix} \mathbf{Z}_{\Gamma\Gamma}^{(s,n)} & \mathbf{Z}_{\Gamma\Xi}^{(s,n)} \\ \mathbf{Z}_{\Xi\Gamma}^{(s,n)} & \mathbf{Z}_{\Xi\Xi}^{(s,n)} \end{bmatrix} \qquad \text{where} \qquad \mathbf{Z}^{(s,n)} = \mathbf{M}^{(\text{blade})}, \mathbf{M}^{(\text{disk})}, \mathbf{K}^{(\text{blade},n)}\left(\Omega\right), \mathbf{K}^{(\text{disk},n)}\left(\Omega\right)\,. \tag{5}$$

In the following simulations, the parameter n refers to different rotational speeds of the bladed disk. To verify the extended modeling approach, a speed range from 0 rpm up to 15,000 rpm is chosen. The samples for the stiffness matrix $\mathbf{K}^{(s,n)}$ are taken at rotational speeds of 0 rpm ($n = 0$), 6,000 rpm ($n = 1$), and 12,000 rpm ($n = 2$, see section 4). This range of the parameter Ω is wide enough to induce distinct changes in eigenfrequencies and eigenvectors by stress stiffening and spin softening.

According to the fixed-interface approach by Craig and Bampton (1968), the vibrational displacement of each component is approximated by a set of dynamic *component modes* $\mathbf{\Phi}^{(s,n)}$ related to the eigenvalues along the diagonal of the spectral matrix $\mathbf{\Lambda}^{(s,n)}$ and static *constraint modes* $\mathbf{\Psi}^{(s,n)}$,

$$\mathbf{K}_{\Xi\Xi}^{(s,n)}\mathbf{\Phi}^{(s,n)} = \mathbf{M}_{\Xi\Xi}\mathbf{\Phi}^{(s,n)}\mathbf{\Lambda}^{(s,n)} \qquad \text{and} \qquad \mathbf{\Psi}^{(s,n)} = -{\mathbf{K}_{\Xi\Xi}^{(s,n)}}^{-1}\mathbf{K}_{\Xi\Gamma}^{(s,n)}\,. \tag{6}$$

By reducing the amount of retained component modes $\mathbf{\Phi}^{(s,n)}$ in the transformation matrix $\mathbf{T}_\mathrm{cms}^{(s,n)}$, a low order modal representation for each component s is obtained,

$$\begin{pmatrix} \mathbf{u}_\Gamma^{(s,n)} \\ \mathbf{u}_\Xi^{(s,n)} \end{pmatrix} = \mathbf{T}_\mathrm{cms}^{(s,n)} \begin{pmatrix} \mathbf{u}_\Gamma^{(s,n)} \\ \boldsymbol{\eta}^{(s,n)} \end{pmatrix} \qquad \text{where} \qquad \mathbf{T}_\mathrm{cms}^{(s,n)} = \begin{bmatrix} \mathbf{I} & \mathbf{0} \\ \mathbf{\Psi}^{(s,n)} & \mathbf{\Phi}^{(s,n)} \end{bmatrix}\,. \tag{7}$$

Subsequent to the transformation in Eq. (7), the disk and blading are reassembled along the interface Γ yielding a reduced order model of the completely bladed disk. Mode-specific frequency mistuning is directly applied to the reduced spectral matrix of each blade.

At this point it should be noted that the transformation matrix $\mathbf{T}_\mathrm{cms}^{(s,n)}$ in Eq. (7) includes mode sets $\mathbf{\Phi}^{(s,n)}$ and $\mathbf{\Psi}^{(s,n)}$ which in turn are dependent on the stiffness matrix $\mathbf{K}^{(s,n)}$. Since a change in rotational speed Ω leads to a stiffness variation, the eigenproblem in Eq. (6) has to be solved for each operating point n.

2.2 Wave-Based Substructuring

After the CMS transformation, the internal displacement $\mathbf{u}_{\Xi}^{(s,n)}$ is represented by a reduced amount of generalized coordinates $\boldsymbol{\eta}^{(s,n)}$. The amount of interface degrees of freedom $\mathbf{u}_{\Gamma}^{(s,n)}$, however, remains unreduced in the model. Therefore, a limited modal basis $\mathbf{W}^{(n)}$ of orthogonal displacement *waves* along the blade-disk-boundary is extracted from a modal analysis of the tuned CMS-reduced blisk model,

$$\begin{pmatrix}\mathbf{u}_{\Gamma}\\ \mathbf{u}_{\Xi}\end{pmatrix} = \begin{bmatrix}\mathbf{I} & \mathbf{0}\\ \boldsymbol{\Psi}^{(n)} & \boldsymbol{\Phi}^{(n)}\end{bmatrix} \mathbf{T}_{\mathrm{wbs}}^{(n)} \begin{pmatrix}\boldsymbol{\xi}^{(n)}\\ \boldsymbol{\eta}^{(n)}\end{pmatrix} \qquad \text{where} \qquad \mathbf{T}_{\mathrm{wbs}}^{(n)} = \begin{bmatrix}\mathbf{W}^{(n)} & \mathbf{0}\\ \mathbf{0} & \mathbf{I}\end{bmatrix}. \tag{8}$$

The orthonormalization of the interface modes $\boldsymbol{\Phi}^{(n)}$ is achieved by a *Singular Value Decomposition* (SVD) as described by Donders (2008) and Hohl et al. (2009),

$$\boldsymbol{\Phi}^{(n)} = \mathbf{Q}^{(n)}\boldsymbol{\Sigma}^{(n)}{\mathbf{V}^{(n)}}^{\mathrm{T}} \qquad \text{and} \qquad \mathbf{W}^{(n)} = \left\{\mathbf{q}_i^{(n)}\right\} \qquad \text{for} \qquad \sigma_i^{(n)} \geq \sigma_{\mathrm{tol}}^{(n)}. \tag{9}$$

The symbol $\boldsymbol{\Sigma}^{(n)}$ denotes a rectangular matrix, while $\mathbf{Q}^{(n)}$ and ${\mathbf{V}^{(n)}}^{\mathrm{T}}$ depict unitary matrices formed column-wise by the left-singular and right-singular eigenvectors of the matrix $\boldsymbol{\Phi}^{(n)}$. Each column $\mathbf{q}_i^{(n)}$ of the matrix $\mathbf{Q}^{(n)}$ represents an orthogonal basis function and is associated to a singular value $\sigma_i^{(n)}$. Based on a tolerance $\sigma_{\mathrm{tol}}^{(n)}$, the amount of column vectors is reduced and the wave basis $\mathbf{W}^{(n)}$ is obtained (see section 3.5). Again, the matrix $\mathbf{T}_{\mathrm{wbs}}^{(n)}$ in Eq. (8) depends on the operating point n and has to be adapted to each rotational speed Ω.

2.3 Secondary Modal Truncation

The last reduction step is based on a modal analysis of the CMS/WBS-reduced model (superscript *). By retaining a limited set of blisk modes $\boldsymbol{\Phi}^{(n)^*}$ in the matrix $\mathbf{T}_{\mathrm{smt}}^{(n)}$, the transformation to the final modal subspace is achieved,

$$\mathbf{u}_{\mathrm{cms,wbs}}^{(n)} = \mathbf{T}_{\mathrm{smt}}^{(n)}\boldsymbol{\eta}^{(n)} \qquad \text{where} \qquad \mathbf{T}_{\mathrm{smt}}^{(n)} = \boldsymbol{\Phi}^{(n)} \qquad \text{and} \qquad \mathbf{K}^{(n)}\boldsymbol{\Phi}^{(n)^*} = \mathbf{M}\boldsymbol{\Phi}^{(n)^*}\boldsymbol{\Lambda}^{(n)^*}. \tag{10}$$

As outlined in the preceding sections, the *Secondary Modal Truncation* (SMT) in Eq. (10) requires repetitive modal analyses at each operating point n.

3 Multi-model Extension

To account for the rotation-induced variation of the mode shapes, the modal bases for the CMS, WBS, and SMT transformation have to be adapted to each operating point of interest. In order to avoid a repetitious passing through the full reduction process for each rotational speed, the modal bases are enriched by mode samples at various operating points. For this purpose, each reduction step is reformulated in terms of a multi-model approach proposed by Balmès (1996), Sternchüss and Balmès (2008), and Sternchüss (2009). In summary, the procedure comprises the following steps:

1. Enrich the modal basis by adding mode samples at various operating points in the relevant speed range.
2. Orthonormalize the enriched modal basis by means of a Singular Value Decomposition.
3. Reduce the dimension of the orthonormal basis by retaining a limited subset of relevant modes.

Following these general steps, the detailed reformulation of the CMS, WBS, and SMT transformation is outlined in the following sections. To account for the stiffness variation by centrifugal forces, a second-order approximation of the reduced stiffness matrix is applied.

3.1 Interpolation of the Stiffness Matrix

Besides the change in mode shapes, the change of the structural eigenfrequencies has to be taken into account. The eigenfrequencies of a rotating bladed disk may either increase (*stress stiffening*) or decrease (*spin softening*)

with rotational speed. To this end, the following interpolation of the reduced spectral matrix $\mathbf{K}_{\text{rom}}$ is applied (Sternchüss, 2009),

$$\mathbf{K}_{\text{rom}}\left(\Omega\right) = \sum_{n=0}^{2} \Omega^{2n} \mathbf{P}_{\text{rom}}^{(n)} = \mathbf{P}_{\text{rom}}^{(0)} + \Omega^2 \mathbf{P}_{\text{rom}}^{(1)} + \Omega^4 \mathbf{P}_{\text{rom}}^{(2)} \,. \tag{11}$$

In the present study, a fourth-order polynomial in rotational speed Ω (upper limit $n_{\max} = 2$) is sufficient to represent both stiffening and softening effects. The coefficient matrices $\mathbf{P}_{\text{rom}}^{(n)}$ are obtained from three samples of reduced stiffness matrices $\mathbf{K}_{\text{rom}}^{(n)}$ at various rotational speeds Ω. In combination with the enriched reduction bases presented in the following sections, the interpolation in Eq. (11) allows an efficient vibration prediction at constant and variable rotational speed. It should be noted that this interpolation may be performed at any reduction level. Since the reduced stiffness matrix features the smallest dimension after CMS, WBS, and SMT transformation, the interpolation is preferably performed at this final stage of the reduction process.

3.2 Extended Component Mode Synthesis

According to section 2.1, the enriched CMS basis is formed by dynamic component modes $\mathbf{\Phi}^{(s,n)}$ and static constraint modes $\mathbf{\Psi}^{(s,n)}$ at various operating points. With respect to the second order polynomial in Eq. (11), three sets of modal samples are used,

$$\mathbf{T}_{\text{cms}}^{(s)} = \begin{bmatrix} \mathbf{I} & \mathbf{0} & \mathbf{I} & \mathbf{0} & \mathbf{I} & \mathbf{0} \\ \mathbf{\Psi}^{(s,0)} & \mathbf{\Phi}^{(s,0)} & \mathbf{\Psi}^{(s,1)} & \mathbf{\Phi}^{(s,1)} & \mathbf{\Psi}^{(s,2)} & \mathbf{\Phi}^{(s,2)} \end{bmatrix} . \tag{12}$$

Relating the additional static modes to a reference modal set $\mathbf{\Psi}^{(s,0)}$, the transformation matrix $\tilde{\mathbf{T}}_{\text{cms}}^{(s)}$ becomes,

$$\begin{aligned} \tilde{\mathbf{T}}_{\text{cms}}^{(s)} &= \begin{bmatrix} \tilde{\mathbf{T}}_{\text{i}}^{(s)} & \tilde{\mathbf{T}}_{\text{m}}^{(s)} \end{bmatrix} \quad \text{where} \quad \tilde{\mathbf{T}}_{\text{i}}^{(s)} = \begin{bmatrix} \mathbf{I} \\ \mathbf{\Psi}^{(s,0)} \end{bmatrix} \quad \text{and} \\ \tilde{\mathbf{T}}_{\text{m}}^{(s)} &= \begin{bmatrix} \mathbf{0} & \mathbf{0} & \mathbf{0} & \mathbf{0} & \mathbf{0} \\ \mathbf{\Psi}^{(s,1)} - \mathbf{\Psi}^{(s,0)} & \mathbf{\Psi}^{(s,2)} - \mathbf{\Psi}^{(s,0)} & \mathbf{\Phi}^{(s,0)} & \mathbf{\Phi}^{(s,1)} & \mathbf{\Phi}^{(s,2)} \end{bmatrix} . \end{aligned} \tag{13}$$

Next, the obtained modal basis is orthonormalized by a Singular Value Decomposition and reduced by retaining only modes associated to singular values above a tolerance $\sigma_{\text{tol}}^{(s)}$,

$$\tilde{\mathbf{T}}_{\text{m}}^{(s)} = \mathbf{Q}^{(s)} \mathbf{\Sigma}^{(s)} {\mathbf{V}^{(s)}}^{\text{T}} \qquad \text{and} \qquad \tilde{\mathbf{T}}_{\text{m,red}}^{(s)} = \left\{ \mathbf{q}_i^{(s)} \right\} \qquad \text{for} \qquad \sigma_i^{(s)} \geq \sigma_{\text{tol}}^{(s)} \,. \tag{14}$$

A synthesis of the reduced basis $\tilde{\mathbf{T}}_{\text{m,red}}^{(s)}$ and its reference $\tilde{\mathbf{T}}_{\text{i}}^{(s)}$ leads to the enriched transformation matrix $\tilde{\mathbf{T}}_{\text{cms,red}}^{(s)}$,

$$\tilde{\mathbf{T}}_{\text{cms,red}}^{(s)} = \begin{bmatrix} \tilde{\mathbf{T}}_{\text{i}}^{(s)} & \tilde{\mathbf{T}}_{\text{m,red}}^{(s)} \end{bmatrix} . \tag{15}$$

3.3 Extended Wave-Based Substructuring

Enriching the set of interface waves in Eq. (8) with samples at different rotational speeds

$$\mathbf{T}_{\text{wbs}} = \begin{bmatrix} \mathbf{W}^{(0)} & \mathbf{0} & \mathbf{W}^{(1)} & \mathbf{0} & \mathbf{W}^{(2)} & \mathbf{0} \\ \mathbf{0} & \mathbf{I} & \mathbf{0} & \mathbf{I} & \mathbf{0} & \mathbf{I} \end{bmatrix} \tag{16}$$

and performing the rearrangement

$$\tilde{\mathbf{T}}_{\text{wbs}} = \begin{bmatrix} \tilde{\mathbf{T}}_{\text{m}} & \tilde{\mathbf{T}}_{\text{i}} \end{bmatrix} \quad \text{where} \quad \tilde{\mathbf{T}}_{\text{m}} = \begin{bmatrix} \mathbf{W}^{(0)} & \mathbf{W}^{(1)} & \mathbf{W}^{(2)} \\ \mathbf{0} & \mathbf{0} & \mathbf{0} \end{bmatrix} \qquad \text{and} \qquad \tilde{\mathbf{T}}_{\text{i}} = \begin{bmatrix} \mathbf{0} \\ \mathbf{I} \end{bmatrix} \tag{17}$$

yields the reduced WBS matrix $\tilde{\mathbf{T}}_{\text{wbs,red}}$,

$$\tilde{\mathbf{T}}_{\text{wbs,red}} = \begin{bmatrix} \tilde{\mathbf{T}}_{\text{m,red}} & \tilde{\mathbf{T}}_{\text{i}} \end{bmatrix} \quad \text{where} \quad \tilde{\mathbf{T}}_{\text{m}} = \mathbf{Q}\mathbf{\Sigma}\mathbf{V}^{\text{T}} \quad \text{and} \quad \tilde{\mathbf{T}}_{\text{m,red}} = \{\mathbf{q}_i\} \quad \text{for} \quad \sigma_i \geq \sigma_{\text{tol}} \,. \tag{18}$$

3.4 Extended Secondary Modal Truncation

Modal analyses of the reduced blisk model at three different rotational speeds provide the SMT basis

$$\mathbf{T}_{\mathrm{smt}} = \begin{bmatrix} \mathbf{\Phi}^{(0)^*} & \mathbf{\Phi}^{(1)^*} & \mathbf{\Phi}^{(2)^*} \end{bmatrix} \qquad \text{where} \qquad \tilde{\mathbf{T}}_{\mathrm{smt}} = \tilde{\mathbf{T}}_{\mathrm{m}} \tag{19}$$

which is orthonormalized and reduced to form the enriched SMT matrix $\tilde{\mathbf{T}}_{\mathrm{smt,red}}$,

$$\tilde{\mathbf{T}}_{\mathrm{smt,red}} = \tilde{\mathbf{T}}_{\mathrm{m,red}} \qquad \text{where} \qquad \tilde{\mathbf{T}}_{\mathrm{m}} = \mathbf{Q}\mathbf{\Sigma}\mathbf{V}^{\mathrm{T}} \qquad \text{and} \qquad \tilde{\mathbf{T}}_{\mathrm{m,red}} = \{\mathbf{q}_i\} \qquad \text{for} \qquad \sigma_i \geq \sigma_{\mathrm{tol}}\,. \tag{20}$$

3.5 Singular Value Tolerance

To illustrate the feasible range of the parameter σ_{tol}, the singular values for a bladed disk at different rotational speeds Ω are analyzed. The effect of choosing a specific tolerance is assessed in terms of the maximum relative difference $\Delta f_{\mathrm{rel,max}}$ of the lowest 100 eigenfrequencies f_i between the reduced and full finite element model,

$$\Delta f_{\mathrm{rel,max}} = \max \left\{ \frac{f_{\mathrm{rom},i} - f_{\mathrm{full},i}}{f_{\mathrm{full},i}} \right\}. \tag{21}$$

In the following, the singular values $\sigma_i^{(n)}$ of the interface waves in Eq. (9) are presented. For simplicity, the values $\tilde{\sigma}_i^{(n)}$ are normalized with respect to the largest singular value $\sigma_1^{(n)}$,

$$\tilde{\sigma}_i^{(n)} = \frac{\sigma_i^{(n)}}{\sigma_1^{(n)}}\,. \tag{22}$$

Despite different operating points n, a similar decrease of the singular values for the analyzed rotational speeds of 0 rpm, 6,000 rpm, and 12,000 rpm is shown in Fig. 1. Consequently, a common tolerance $\tilde{\sigma}_{\mathrm{tol}}^{(n)} = 0.1$ is chosen for all three angular velocities. Exemplary values for some tolerance levels are listed in Tab. 1.

Table 1: Maximum relative frequency difference $\Delta f_{\mathrm{rel,max}}$ between ROM and FEA as a function of the normalized singular value tolerance $\tilde{\sigma}_{\mathrm{tol}}^{(n)}$

Tolerance $\tilde{\sigma}_{\mathrm{tol}}^{(n)}$	Interface waves i	Max. frequency difference $\Delta f_{\mathrm{rel,max}}$
0.1	100 waves	$< 2\%$
0.3	75 waves	$< 5\%$
0.7	20 waves	$< 10\%$

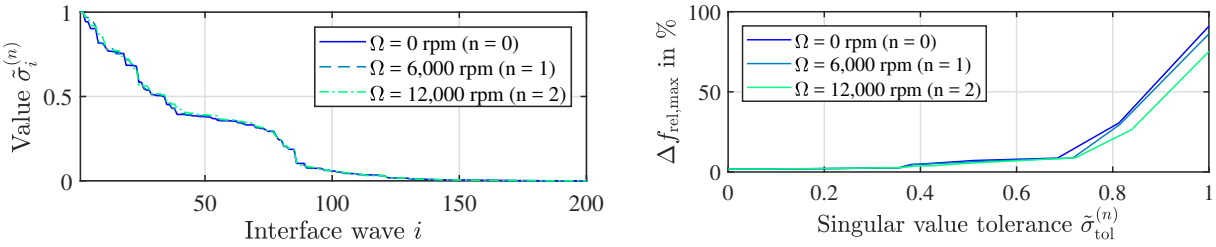

Figure 1: Normalized singular values $\tilde{\sigma}$ of the interface waves (left) and maximum frequency difference $\Delta f_{\mathrm{rel,max}}$ between the FEA and ROM with various tolerances $\tilde{\sigma}_{\mathrm{tol}}^{(n)}$ for the first 100 tuned blisk modes (right) at constant rotational speeds Ω of 0 rpm, 6,000 rpm, and 12,000 rpm

4 Comparison with the Full Model

To assess the accuracy of the reformulated modeling approach, the reduced order model of a sample blisk comprising ten bladed segments is compared to its full finite element representation. First, an appropriate discretization of the blisk by finite elements has to be chosen by comparing the results obtained from successively refined meshes. Since this study is focused on modeling the evolution of dynamic properties under rotation, the relative change $\Delta f_{\mathrm{rpm},k}$ of the eigenfrequency f_k in the speed range from $\Omega_{\min}$ = 0 rpm up to $\Omega_{\max}$ = 15,000 rpm is chosen as a convergence criterion between the meshes,

$$\Delta f_{\mathrm{rpm},k} = \left\| \frac{f_k\left(\Omega_{\max}\right) - f_k\left(\Omega_{\min}\right)}{f_k\left(\Omega_{\min}\right)} \right\| . \tag{23}$$

The results of the mesh convergence study in Fig. 2 indicate that the maximum frequency change $\Delta f^{\max}_{\mathrm{rpm},k}$ of about 70% in the analyzed speed range is well predicted by meshes with at least 5,000 *degrees of freedom* (dof). A detailed study of 10 mode families with two nodal diameters shows that the maximum frequency change $\Delta f^{\mathrm{ND2}}_{\mathrm{rpm},k}$ is related to the first mode family. In view of the computational expense to solve the unreduced finite element model, a medium mesh size with 9,300 dof is chosen for the subsequent model verification.

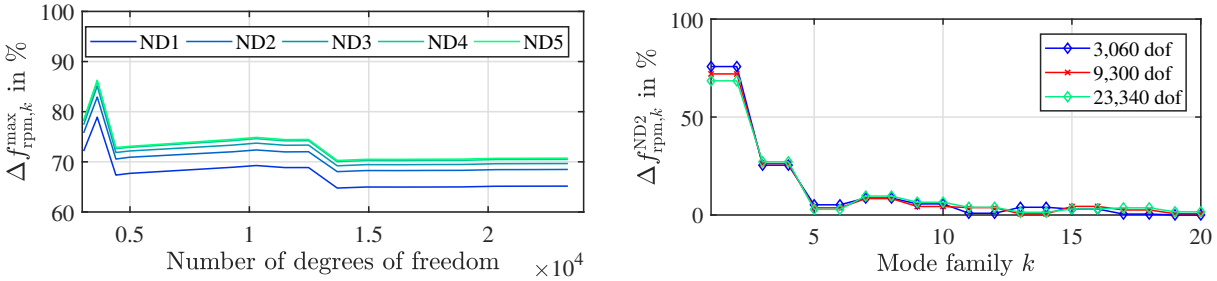

Figure 2: Relative change $\Delta f_{\mathrm{rpm},k}$ of eigenfrequencies in the rotational speed range from 0 rpm to 15,000 rpm for different finite element meshes and various nodal diameters ND

The comparison between the reduced and full model in Fig. 3 is performed at different steady operating points with constant rotational speeds. The reduced order approximation is based on three samples of prestressed stiffness matrices at speeds Ω of 0 rpm, 6,000 rpm, and 12,000 rpm. The number of retained modes in the enriched CMS, WBS, and SMT bases is listed in Tab. 2. Prior to addressing a mistuned configuration under rotation, the tuned dynamics of the blisk are discussed. In conclusion, the effectiveness of the presented approach in terms of computational time saving is highlighted.

Table 2: Parameters of the reduced order model

CMS	WBS	SMT
10 modes per blade / 10 modes per harm. index	200 waves	100 blisk modes

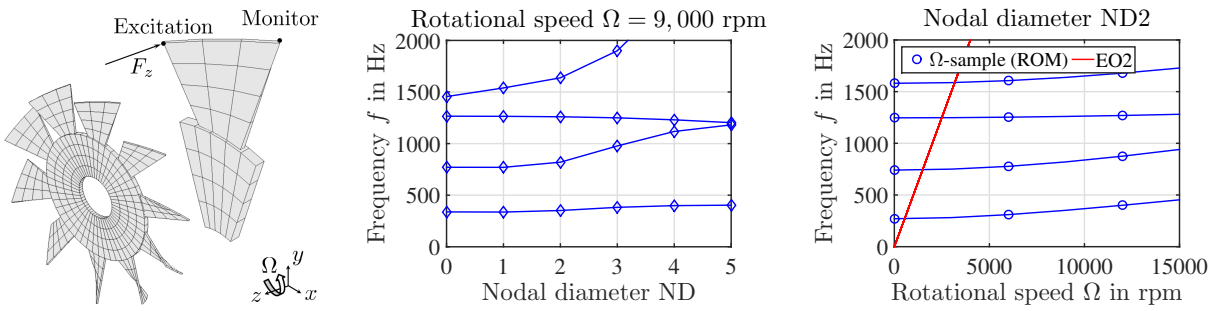

Figure 3: Finite element model, nodal diameter diagram, and ND2-Campbell diagram of the tuned blisk (stiffness samples for ROM taken at constant rotational speeds Ω of 0 rpm, 6,000 rpm, and 12,000 rpm)

4.1 Tuned Blisk under constant Rotation

First, the mode shape approximation by enriched CMS, WBS, and SMT bases is evaluated in terms of the *Modal Assurance Criterion* (MAC) presented by Allemang and Brown (1982). The interpolation of the reduced stiffness matrix within a limited range of rotational speeds is rated by means of the relative eigenfrequency difference Δf_{rel} between the reduced and full finite element model,

$$\text{MAC}_{i,j} = \frac{|\boldsymbol{\Phi}_{\text{rom},i}^{\text{T}} \boldsymbol{\Psi}_{\text{full},j}|^2}{\boldsymbol{\Phi}_{\text{rom},i}^{\text{T}} \boldsymbol{\Phi}_{\text{rom},i} \boldsymbol{\Psi}_{\text{full},j}^{\text{T}} \boldsymbol{\Psi}_{\text{full},j}} \qquad \text{and} \qquad \Delta f_{\text{rel},i} = \frac{f_{\text{rom},i} - f_{\text{full},i}}{f_{\text{full},i}} \,. \tag{24}$$

Since slight frequency differences between the full and reduced order models may lead to a different order of the associated mode shapes i, the resulting modal assurance criterion $\text{MAC}_{i,i}$ undergoes abrupt changes between maximum and minimum values. This circumstance is illustrated by a progressively increasing scatter of large MAC values for higher modes in the contour plot of Fig. 4.

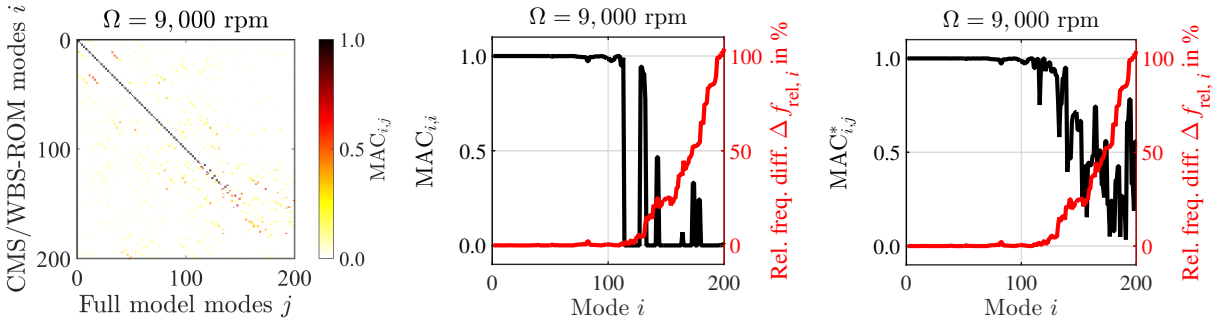

Figure 4: Modal assurance criteria and relative frequency differences of the tuned blisk for a constant rotational speed of 9,000 rpm

Consequently, a modified criterion $\text{MAC}^*_{i,j}$ is defined which yields a gradually decreasing mode correlation for increasing frequency deviations in Fig. 4,

$$\text{MAC}^*_{i,j} = \max_j \left\{ \frac{|\boldsymbol{\Phi}_{\text{rom},i}^{\text{T}} \boldsymbol{\Psi}_{\text{full},j}|^2}{\boldsymbol{\Phi}_{\text{rom},i}^{\text{T}} \boldsymbol{\Phi}_{\text{rom},i} \boldsymbol{\Psi}_{\text{full},j}^{\text{T}} \boldsymbol{\Psi}_{\text{full},j}} \right\} . \tag{25}$$

The accuracy of the parameterized multi-model formulation is assessed at the sample speeds of 0 rpm, 6,000 rpm, and 12,000 rpm as well as intermediate and extended speeds of 3,000 rpm, 9,000 rpm, and 15,000 rpm. A MAC level above 0.96 and a relative frequency difference below 1% for the first 110 modes in Fig. 5 demonstrates the accurate approximation of free blisk vibrations at different rotational speeds by the reduced order model. While this decent approximation is expected for operating points which are included as stiffness samples in the model, the good correlation at intermediate and extrapolated rotation speeds demonstrates the validity of the underlying stiffness interpolation in Eq. (11) and the multi-model extension.

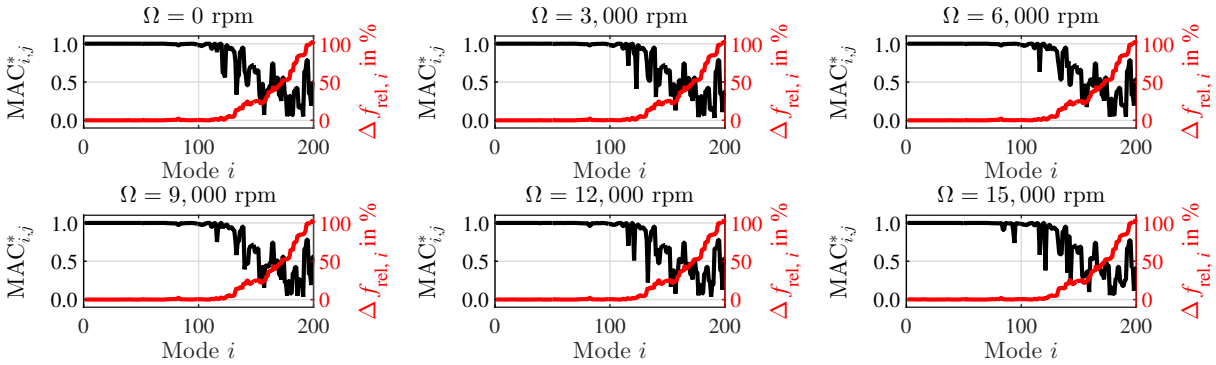

Figure 5: Modal assurance criteria and relative frequency differences of the tuned blisk for constant rotational speeds ranging from 0 rpm to 15,000 rpm

This conclusion is substantiated by the excellent agreement of the forced EO2 response of the full and reduced blisk models at a rotor speed of 9,000 rpm in Fig. 6. The depicted amplitude $\hat{u}^*$ is normalized with respect to the maximum displacement of the tuned blisk at rotor standstill. To illustrate the stiffening effect on the forced response, an amplitude comparison for various rotational speeds is provided in Fig. 7. Again, the amplitudes of the full and reduced order models match well in the analyzed range of frequencies and rotational speeds. A detailed view of the stiffening effect on the resonance of the first flapwise bending mode is provided in Fig. 7.

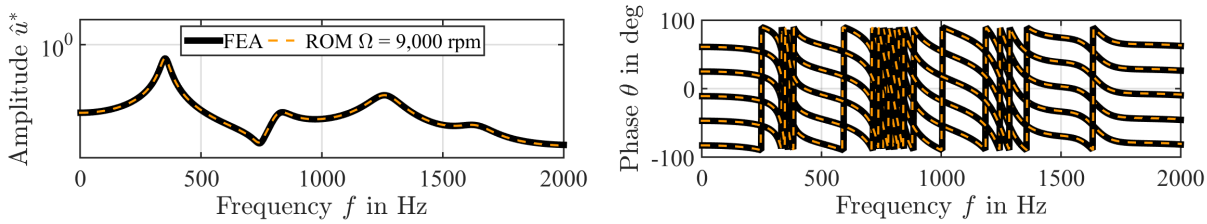

Figure 6: Forced EO2 response of the reduced and full finite element models of the tuned blisk for a constant rotational speed Ω of 9,000 rpm

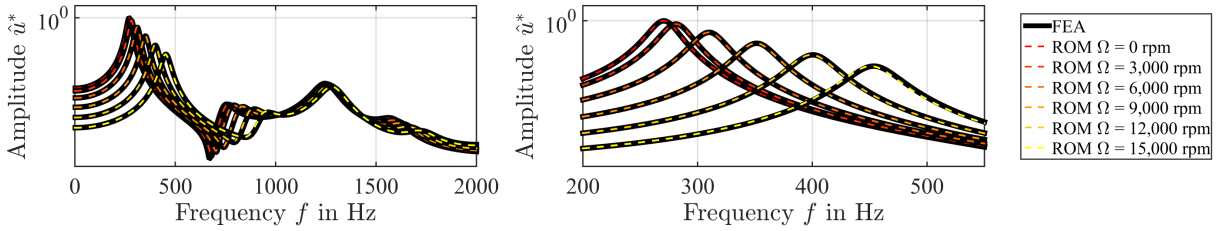

Figure 7: Forced EO2 response of the reduced and full finite element models of the tuned blisk for constant rotational speeds Ω ranging from 0 rpm to 15,000 rpm

4.2 Mistuned Blisk under constant Rotation

To assess the accuracy of the reduced order prediction for mistuned bladed disks, the stiffness of each blade k is multiplied by an individual mistuning factor κ_k in Tab. 3. It should be noted that this frequency mistuning is applied to the blading at rotor standstill. Consequently, the ratios of tuned and mistuned blade frequencies may change for various operating points. In the presented reduced order model, this evolution of mistuning factors with a variable speed Ω is covered by considering the reduced stiffness matrices of each individual blade at three different rotational speeds and applying the interpolation in Eq. (11).
A comparison between the full and reduced models by means of a mistuned EO2 response at 9,000 rpm is presented in Fig. 8. Again, an excellent agreement in terms of amplitude and phase approximation is highlighted. The accuracy of the reduced order model for various rotational speeds ranging from 0 rpm to 15,000 rpm is demonstrated in Fig. 9.

Table 3: Frequency mistuning factors of the blisk at rotor standstill ($\Omega = 0$ rpm)

Blade k	1	2	3	4	5	6	7	8	9	10
κ_k	0.84	0.98	1.05	0.81	1.49	1.05	1.12	0.52	1.41	1.12

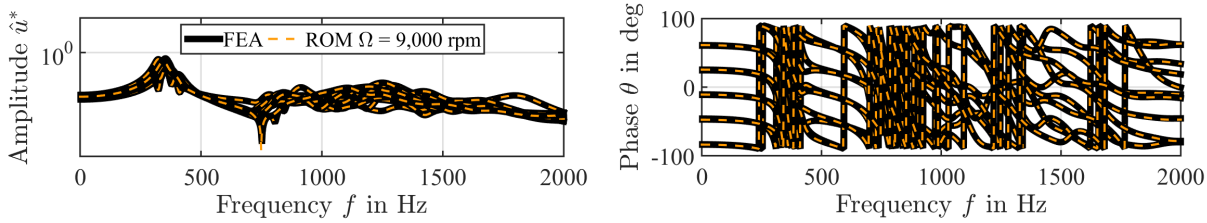

Figure 8: Forced EO2 response of the reduced and full finite element models of the mistuned blisk for a constant rotational speed Ω of 9,000 rpm

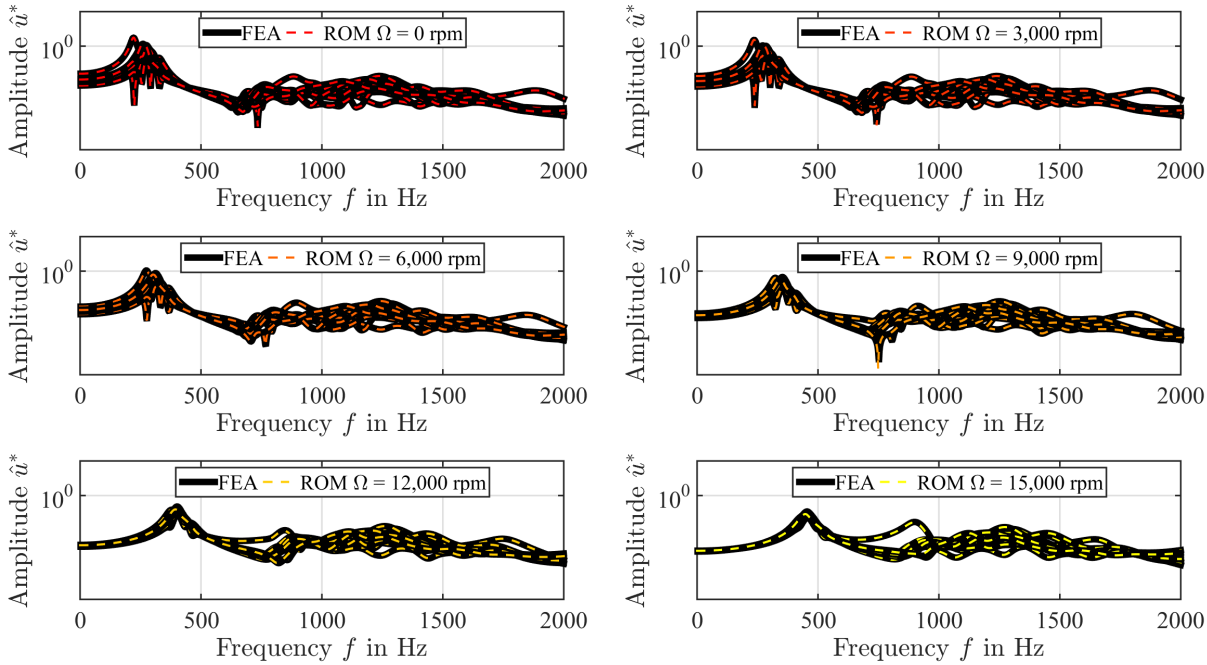

Figure 9: Forced EO2 response of the reduced and full finite element models of the mistuned blisk for constant rotational speeds Ω ranging from 0 rpm to 15,000 rpm

4.3 Computational Time Saving

To highlight the effectiveness of the presented approach, the computational times required for the forced response analysis of the previously introduced blisk sample are shown in Fig. 10. The computational setup used for all simulations is summarized in Tab. 4. First, the time t_{FEA} required for solving the full finite element model is compared to the overall computation time $t_{\text{ROM,total}}$ of the reduced order model (including the model reduction as well as the solution process). This direct comparison demonstrates that the reduced order approach outperforms the full model by a factor of almost four (saving 73% of computational time).
In addition, the amount $t_{\text{ROM,reduction}}$ of 48 s indicates that the reduction process takes up more than half of the overall computation time $t_{\text{ROM,total}}$ of 77 s. Since the model reduction has to be performed just once prior to the actual solution process, the reduced order approach provides a computational saving of 90% for the forced response prediction in comparison to the full finite element model.

Table 4: Computational setup used for all simulations

Operating system	CPU	RAM
Windows 7 Professional (64 Bit)	Intel Core i5-4590 (3.3 GHz)	16 GB

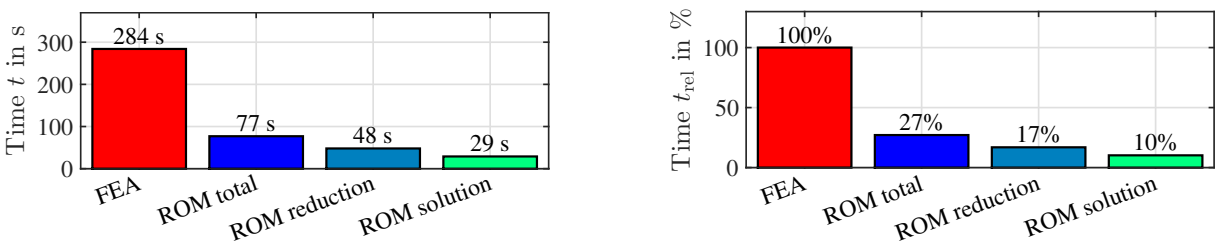

Figure 10: Comparison of the computational time required for a mistuned forced response prediction (1,000 frequency samples per response curve) by the full finite element model and the reduced order approach

5 Analysis of Blisks under variable Rotation

Besides the vibration prediction for various constant operating points, the presented model allows the analysis of bladed disks at variable speeds of rotation. In the following, the resonance of the first flapwise bending mode for a synchronous stimulus according to Eq. (4) is analyzed. Since each frequency f is related to a specific rotational speed Ω via the engine order EO, the structural properties are adapted to each operating point in the analyzed frequency range according to Eq. (11). It should be noted that despite the variation of rotor speed, the response at each frequency is assumed as a steady operating state and no transient run-up or coast-down effects are considered. In Fig. 11, the forced response of the tuned blisk under variable rotor speed (indicated by the tilted line) is compared to its amplitudes at constant rotation for the engine orders EO2, EO6, and EO10. It becomes clear that the frequencies at the crossings of the synchronous response (tilted line) and the amplitudes at constant rotation meet the condition in Eq. (4) according to the specific engine order. For example, the amplitude response at 15,000 rpm (corresponding to $\Omega = 250$ Hz) is crossed by the variable EO2 response at a frequency f of 500 Hz. In addition, the stiffening effect modeled by Eq. (11) is identifiable as an increase of the resonance frequency with growing rotor speed.

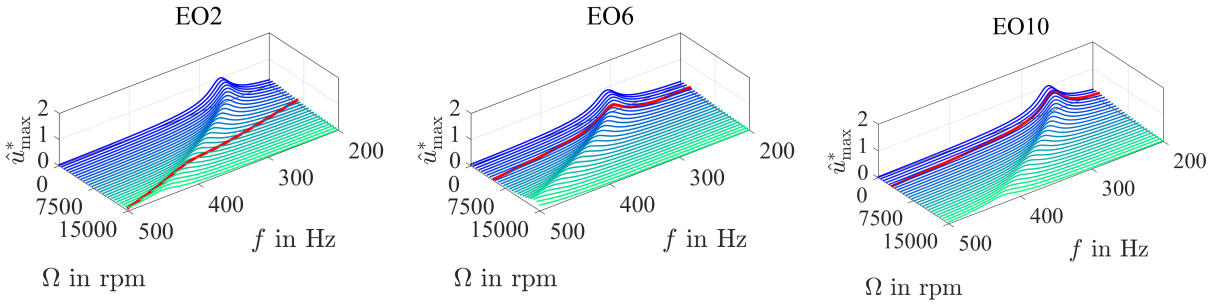

Figure 11: Forced response of the tuned reduced order model for constant and variable rotational speeds (tilted line)

A comparison between the forced EO2, EO6, and EO10 responses of a mistuned blisk (see Tab. 3) under variable rotation and its responses at constant rotational speed is shown in Fig. 12. For simplicity, the mistuned response is depicted in terms of the overall envelope of the maximum amplitudes. Again, the response crossings for variable and constant rotational speeds meet the relation in Eq. (4).

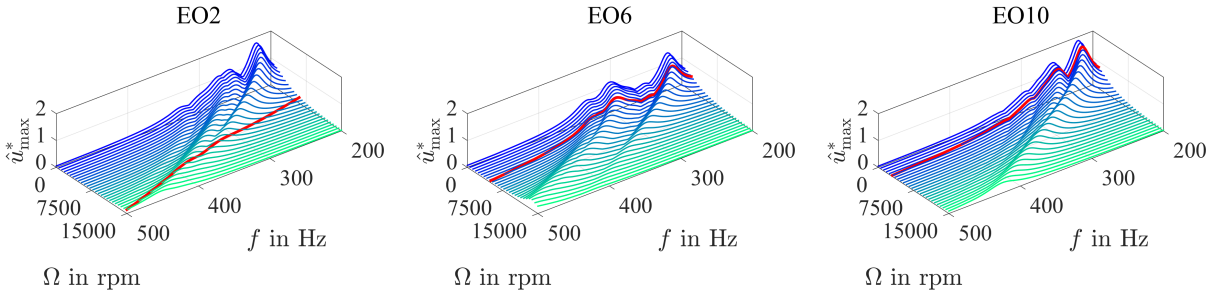

Figure 12: Maximum amplitudes of the mistuned reduced model for constant and variable rotor speeds (tilted line)

To study the effect of constant and variable rotor speed Ω on the amplification of mistuned vibrations, the following ratio between the maximum amplitude of the tuned (superscript $^{\text{tu}}$) and mistuned blisk (superscript $^{\text{mt}}$) is defined:

$$a_\Omega = \frac{\hat{u}_\Omega^{\text{mt,max}}}{\hat{u}_\Omega^{\text{tu,max}}} \,. \tag{26}$$

While the maximum amplitude ratio at constant rotational speed is obtained by division of the amplitude maxima along the response curves aligned with the frequency abscissa f in Fig. 11 and Fig. 12, the amplification factor a_Ω under variable rotation results from the ratio of the tilted response curves in mentioned figures. It should be noted that the frequency range which is considered for the determination of the maximum amplitudes $\hat{u}_\Omega^{\max}$ under variable rotation depends on the actual rotor speed Ω and the analyzed engine order EO through Eq. (4). Consequently, the analysis of EO1 is limited to excitation frequencies below 250 Hz since this value corresponds to the upper limit of the rotational speed range ($\Omega = 15{,}000$ rpm) validated in section 4.

The corresponding amplification factors for engine orders EO1 to EO10 are depicted in Fig. 13. It is indicated that the amplitude amplification ratios for all analyzed engine orders at constant rotor speed tend to decrease for an increase in Ω. This result is in accordance with the mitigation effect of rotation on mistuning reported by Moyroud et al. (2002) and Nipkau (2011).

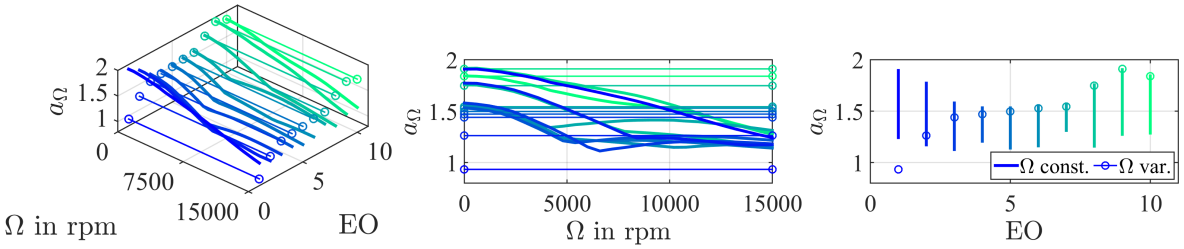

Figure 13: Amplitude amplification of the mistuned reduced order model for constant and variable rotational speed

In comparison, the maximum amplitude amplification for engine orders EO5 to EO10 under variable rotor speed (indicated by circles in Fig. 13) is of the same order as the ratios at constant rotational speed. For EO1 to EO4 the assumption of constant rotational speed leads to an overprediction of the mistuning effect. This result can be traced back to Eq. (4), Fig. 11, and Fig. 12: Since the synchronous stimulus response (tilted line) approaches the response at rotor rest ($\Omega = 0$ rpm, line aligned with frequency axis) for large EO levels, the amplitude amplification for an increasing engine order converges towards the corresponding maximum value at rotor standstill.

6 Summary and future Work

The extension of a reduced order model to account for the rotational speed dependence of mistuned bladed disk dynamics has been presented. By usage of a multi-model formulation presented in Balmès (1996), Sternchüss and Balmès (2008), and Sternchüss (2009), the reformulated substructural approach allows efficient blade vibration predictions at constant and variable rotor speeds. The accuracy of the model has been demonstrated in terms of modal assurance criteria, relative frequency differences, and a forced response comparison. Comparing the computational times for solving the reduced model and the full finite element representation of a mistuned blisk reveals a time saving of 90%. The applicability of the proposed approach has been shown by the study of a mistuned bladed disk at various rotational speeds. The analyses indicate that the rotational motion has a mitigating effect on the amplitude amplification caused by mistuning.
In future work, the evolution of the speed-dependent mistuning coefficients will be incorporated in the presented model. Finally, the numerically predicted response may be compared to experimental measurements in an operating turbomachinery test rig.

Acknowledgments

This work was supported by the German Research Foundation (DFG) and the Research Association for Combustion Engines (FVV) e.V. within the framework of the co-funded project “Mistuning of bladed disks with aerodynamic and structural coupling”.

References

Allemang, R. J.; Brown, D. L.: A Correlation Coefficient for Modal Vector Analysis. In: *Proceedings of the 1st International Modal Analysis Conference*, pages 110–116 (1982).

Balmès, E.: Parametric families of reduced finite element models. Theory and applications. In: *Mechanical Systems and Signal Processing*, vol. 10(4), pages 381–394 (1996).

Craig, R. R.; Bampton, M. C. C.: Coupling of Substructrures for Dynamic Analysis. *AIAA Journal*, , 6, (1968), 1313–1319.

Donders, S.: *Computer-aided engineering methodologies for robust automotive NVH design*. Ph.D. thesis, KU Leuven, Leuven (2008).

Feiner, D. M.: *A Fundamental Model of Mistuning for Forced Response Prediction and System Identification*. Ph.D. thesis, Carnegie Mellon University, Pittsburgh (2002).

Feiner, D. M.; Griffin, J. H.: Mistuning Identification of Bladed Disks Using a Fundamental Mistuning Model - Part I: Theory. *ASME J. Turbomach.*, 126(1), (2004), 150–158.

Hohl, A.; Siewert, C.; Panning, L.; Wallaschek, J.: A Substructure Based Reduced Order Model for Mistuned Bladed Disks. In: *ASME 2009 International Design Engineering Technical Conferences and Computers and Information in Engineering Conference*, pages 899–906 (2009).

Maywald, T.; Beirow, B.; Heinrich, C. R.; Kühhorn, A.: Vacuum Spin Test Series of a Turbine Impeller With Focus on Mistuning and Damping by Comparing Tip Timing and Strain Gauge Results. In: *ASME Turbo Expo 2015: Turbine Technical Conference and Exposition, GT2015-42649* (2009).

Moyroud, F.; Fransson, T.; Jacquet-Richardet, G.: A Comparison of Two Finite Element Reduction Techniques for Mistuned Bladed Disks. *ASME J. Eng. Gas Turbines Power*, 124(4), (2002), 942–952.

Nipkau, J.: *Analysis of Mistuned Blisk Vibrations Using a Surrogate Lumped Mass Model with Aerodynamic Influences*. Ph.D. thesis, Brandenburgische Technische Universität Cottbus, Cottbus (2011).

Sternchüss, A.: *Multi-level parametric reduced order models of rotating bladed disk assemblies*. Ph.D. thesis, École Centrale Paris, Paris (2009).

Sternchüss, A.; Balmès, E.: On the reduction of quasi-cyclic disks with variable rotation speeds. In: *International Conference on Advanced Acoustics and Vibration Engineering*, pages 3925–3939 (2008).

Address: Institute of Dynamics and Vibration Research, Leibniz Universität Hannover, 30167 Hannover, Germany
email: `willeke@ids.uni-hannover.de`